Heat Mass Transfer (2017) 53:2265–2277
DOI 10.1007/s00231-017-1978-7

ORIGINAL

Experimental and numerical investigation of pressure drop and heat transfer coefficient in converging–diverging microchannel heat sink

M. K. Dheepan Chakravarthii[1] · D. Mutharasu[1] · S. Shanmugan[1]

Received: 20 September 2016 / Accepted: 22 January 2017 / Published online: 31 January 2017
© Springer-Verlag Berlin Heidelberg 2017

Abstract The major challenge in microelectronic chips is to eliminate the generated heat for stable and reliable operation of the devices. Microchannel heat sinks are efficient method to dissipate high heat flux. The pressure drop and heat transfer coefficient are the important parameters which determine the thermal–hydraulic performance of the microchannel heat sink. In this study, a converging–diverging (CD) microchannel heat sink was experimentally investigated for the variation of pressure drop and heat transfer coefficient. De-ionized water was considered as the working fluid. Experiments were conducted for single phase fluid flow with mass flow rate and heat flux ranging from 0.001232 to 0.01848 kg/s and 10–50 W/cm^2 respectively. The fluid and solid temperature were measured to calculate the heat transfer coefficients. Numerical results were computed using the CFD software and validated against the experimental results. The CD microchannel possesses high heat transfer coefficient than the straight microchannels. Theoretical correlations were proposed for comparing the experimental Nusselt number of CD microchannel. Evaluation of thermal–hydraulic performance of CD microchannel is important to quantify its applications in electronics cooling.

1 Introduction

With the advancements in aerospace technology, microelectromechanical systems, hybrid data centres and microfluidics, the miniature size electronic chips in such applications are the need of the century. According to the Moore's law, the increase in operating temperature of the electronic boards results in detoriation of component's durability. Also, International technology Roadmap for semiconductors (ITRS, 2009) alarmed that the thermal management in high performace chip packages will be crucial for intermittent and efficient operation of the parent device. Innovative as well as effective thermal solution is demanded by the growing technical advancements. Though the worldwide research has been conducted on different thermal heat dissipation, microchannel heat sinks are very promising in terms of high heat flux dissipation capacity and compatibility with the electronics system. However, the performance of microchannel heat sinks is quite unsatisfactory and lot of research have been done in improving the microchannel system.

The research on Microchannels were began by Tuckerman et al. [1]. Successive researches have been done to increase the heat transfer coefficients using single phase flow in microchannel with different aspect ratio. Singh et al. [2] demonstrated the successful application of microchannel cooling for moderation of high heat flux transients such as p-n diodes, Metal-oxide semiconductor Field-Effect transistor (MOSFET) and resitance termperature detectors (RTDs) [3]. Flow boiling in microchannels displays varying heat distribution in channel walls for constant heat flux boundary at the outer wall of microchannel. The problem of flow boiling, flow reversal, reduced critical heat flux, thermal stresses, pressure and temperature fluctuation in linear microchannels urged for different topology [4–7]. Many researches were done on microchannels with micro pin fins, surface roughness and tortuous channels [4, 8–12]. Nucleate boiling in the above mentioned modifications limits its applications. In general, only sinusoidal wall shape

✉ M. K. Dheepan Chakravarthii
dheepan.mk@gmail.com

[1] Lab 335, School of Physics, Universiti Sains Malaysia, 11800 Gelugor, Penang, Malaysia

were considered in the design of microchannels [12]. Lee and Pan [6] used diverging microchannels to mitigate the effects of flow instablilites that causes nucleate boiling. The presence of critical angle which can reduce the pressure drop in single phase microchannel were reported by [7].

Relatively few studies on the diverging/converging microchannels were done. Liang Gong et al. used microchannel with wavy walls to improve the heat transfer performance in low Reynolds number laminar fluid flow for high heat flux [13]. They reported 55% increase in overall performance in comparison to straight microchannels. Particle motions in converging–diverging microchannels were experimentally investigated by Xiangchun et al. [14]. They studied the motion of polystyrene particles in converging–diverging section of microchannel and partially successful in concluding the dependability of velocity ratio and particle size. Louisos and Hitt [14] and Duryodhan et al. [16] studied the convective heat transfer in diverging and converging microchannels. The dominance of conjugate effect in heat transfer were also reported. Duryodhan et al. [17] proposed a methodology for calculating the characteristic length for varying cross section in microchannels. The selection of hydraulic diameter at the characteristic dimension for the converging/diverging microchannels is important to analyze the flow conditions. In their further studies [18], experimental demonstration of the isothermal wall condition for a constant heat flux condition were developed. Later, two cross sections, converging and diverging as separate microchannels were considered. The pressure drop and Nusselt number were compared in both the models. Yong et al. simulated the heat transfer performance of Microchannels with converging–diverging passages [19]. Their study was validated by calculating the Enhancement factors (En) and performance factor (PF). They reported an overwhelming improvement of thermal–hydraulic performance to 60% in comparison to straight microchannels. In summary, the microchannels with varying cross section increases the heat transfer enhancement in electronic devices with high heat flux applications. The flow instability in the microchannels were reduced thereby reducing the friction factor and increasing the heat transfer coefficient. To the best of author's knowledge, the research involving the converging–diverging microchannels is very minimal. Thorough investigation in converging–diverging microchannels is necessary for its substantial applications.

In this study, a combination of converging and diverging microchannel heat sink were considered. Converging diverging (CD) microchannels were designed by FloEFD 15 and a three-dimensional numerical study was conducted for optimizing the performance of CD microchannel. Experiments were conducted to understand the heat transfer phenomenon in CD microchannel. De-ionized water was used as the working fluid and the measurements were made for heat input and mass flow rate range of 10–50 W/cm^2 and 0.001232–0.01848 kg/s respectively. The pressure drop and heat transfer coefficient were measured and plotted for different correlations. To validate the experimental measurements, CFD simulations were performed. The simulation results were found to be in good agreement with the experimental results.

2 Experimental details

2.1 Experimental setup and procedure

The schematic layout of the experimental setup employed in this study is shown in the Fig. 1 which is similar to that used earlier [18, 27]. The experimental setup consists of fluid tank, pump, flow meter, differential pressure gauge, test section (Microchannel under test and header), heater, digital thermocouples and DC power supply. De-ionized water is used as the working fluid. The pump used is QB-60 whose maximum power is 0.37 kW. A pre-calibrated flow

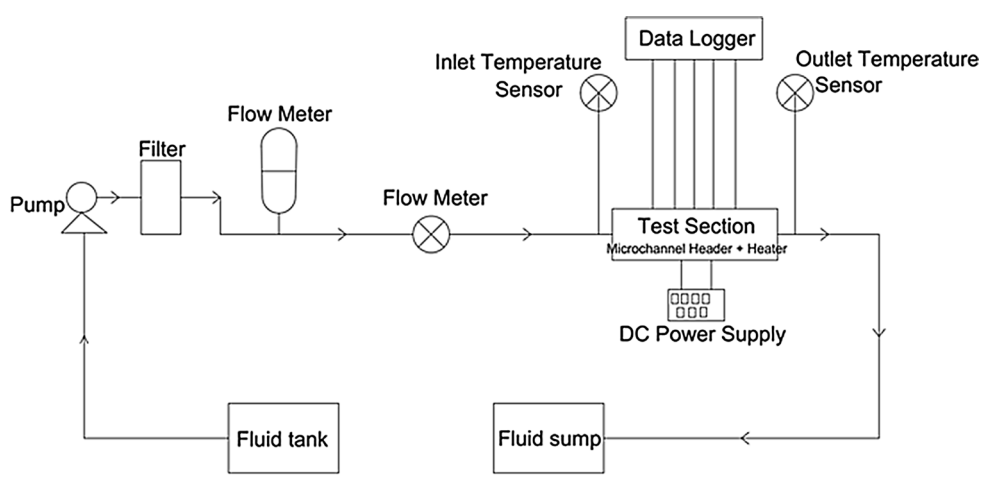

Fig. 1 Schematic layout of experimental setup used in this study

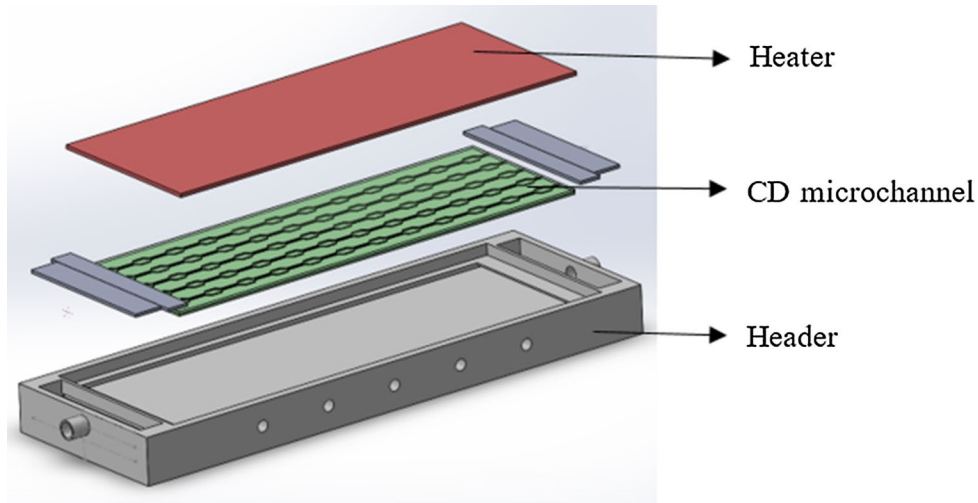

Fig. 2 Exploded assembly view of header, CD microchannel and heater

meter is used to control the mass flow rate of the liquid in the setup. The pre-calibrated pressure gauge is used to measure the pressure across the microchannel. Two digital thermocouples are used to measure the inlet and outlet temperatures on the surface of the microchannel. A custom-made header is designed and manufactured to study the performance of the converging–diverging microchannel. The header have inlet and outlet ports for the fluid to flow in and flow out. The header have 3 mm holes for the thermocouple beads to be slotted for measuring temperature. A 5 W heater is placed on top of the microchannel which acts as the heat source supplying constant heat flux. Insulation is provided between the header and microchannel surface to prevent any sort of heat transfer and unnecessary heat losses. Figure 2 shows the exploded assembly view of the header, CD microchannel heat sink and heater. A DC power supply is connected to the heater for constant power supply. All the devices are connected using Teflon tubing which is capable of withstanding high temperature.

The experimental procedure adopted is similar to that employed by Duryodhan et al. [16]. The de-ionized water was boiled for 30 min to evaporate the dissolved air (if any) and then cooled to room temperature. The fluid tank was filled with the boiled de-ionized water. The pump flow was started and the flow meter has been adjusted to provide a steady flow in the experimental circuit. The input and output temperature of the fluid and the pressure drop was continuously monitored until the flow in the circuit is steady. This means that, the steady state flow was assumed to be achieved when the fluctuation in temperature and pressure drop measurement is almost zero. Once the steady state condtion was achieved, all the required parameters such as flow rate, pressure drop, inlet and outlet temperature, heat flux were measured. Aforementioned procedure was repeated for different measurement conditions.

2.2 Converging–diverging microchannels

The converging–diverging microchannels and straight microchannels employed in this study are shown in the Fig. 3a. The microchannels are designed using Solidworks® software and fabricated by high precision micro-milling machine. Aluminium 5051 material was chosen for this study. The surface roughness of each microchannel was measured using Axio CSM700 Controller Zeiss microscope which posses 10× magnification factor. The average surface roughness of the microchannel was measured to be 0.853 µm. The detailed geometrical specification of the microchannels employed in this study are given in Table 1.

The length (L), width (B) and thickness (t) of the CD microchannel heat sinks are 120, 40 and 1.2 mm respectively. The dimensions of the CD microchannel was optimized for higher heat dissipation. The bigger width and smaller width of CD microchannel dimensions used in this study are 3000 µm (Maximum) and 500 µm (Minimum) with 51.34° converge–diverge angular constraint. For better understanding and easy calculation of aspect ratio and hydraulic diameter, the single unit of CD microchannel was divided into five sections as shown in Fig. 3b. Sections 1 and 5 comprises minimum aspect ratio while the Sect. 3 has maximum aspect ratio. To be noted, Sects. 2 and 3 are the converging and diverging sections respectively and hence possess varying aspect ratio.

2.3 Data reduction

The heat transfer coefficient, Reynolds number and Nusselt number calculation procedures are explained in this section. The heat supplied to the surface of the microchannel is not completely carried away by the flowing water. At the instance of power supply to the heater, the water at the inlet

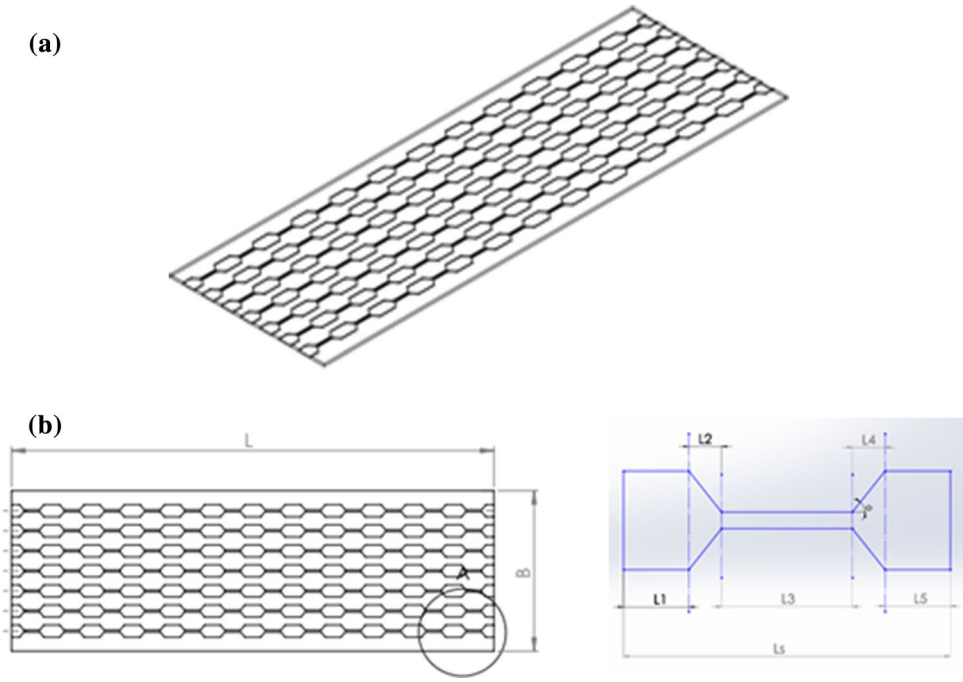

Fig. 3 Microchannel heat sink considered in this study **a** 3D CAD model of CD Microchannel heat sink, **b** 2D Top view of CD Microchannel heat sink with detail A showing Sects. 1, 2, 3, 4 and 5

Table 1 Geometrical parameters

Parameter	Value	Unit
Length of CD microchannel unit	10	mm
Smaller width of CD microchannel unit	500	µm
Bigger width of CD microchannel unit	3000	µm
Converge and diverge angle	51.34	(°)
Hydraulic diamter in converge section	706	µm
Hydraulic diamter in diverge section	727	µm

reservoir utilizes a small fraction of heat. Another fraction of the heat supplied gets dissipated to the ambient air in the surrounding through convection and radiation. Duryodhan et al. conducted a heat loss analysis and reported a maximum of 12% loss to the surrounding in the form of convection and radiation [16]. However, the inclusion of header in this study requires a different heat loss analysis.

The heat loss curve determines the amount of heat lost (Q_{loss}) to the atmosphere. To generate the heat loss curve, the following procedure was adopted. Firstly, power was supplied to the microchannel with no fluid-flow in it and the corresponding surface temperature of the microchannels was measured. Secondly, fluid was allowed to flow at constant flow rate and input power to the heater was adjusted to obtain the same surface temperature as that of no fluid flow. The difference in power obtained against the surface temperature was plotted as heat loss curve as shown in Fig. 4. In this case, the maximum heat loss was found to be 16% for the mass flow rate of 0.01355 kg/s. The increase in mass flow rate reduces the heat loss through convection and radiation.

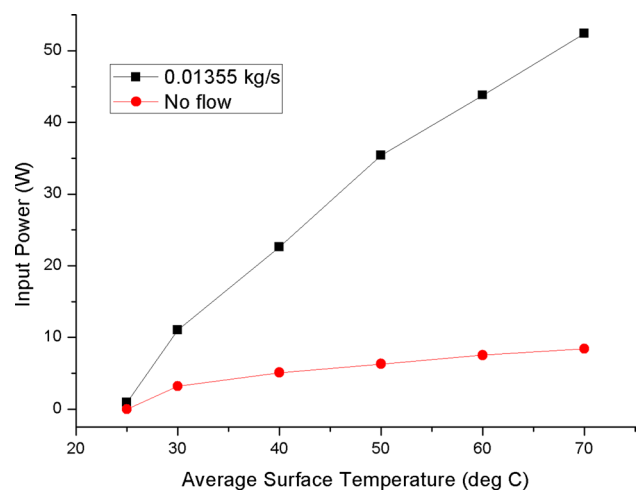

Fig. 4 Heat loss curve for CD microchannel

The following are the equations to determine the heat carried away by the fluid in the microchannels: Total heat in the tank is given by:

$$Q_{tank} = Q_{in} - (Q_{channel} + Q_{loss}) \quad (1)$$

Heat in the channel is calcualted by:

$$Q_{channel} = \dot{m}c_p(T_{out} - T_{in}) \quad (2)$$

The heat carried away by the channel is given by:

$$h_{out} = \frac{Q_{heat}}{(T_f - T_s)} \quad (3)$$

where T_f and T_s is the average fluid temperature and Surface temperature respectively. T_f and T_s are given by:

$$T_f = \frac{T_{fi} + T_{fo}}{2}$$

$$T_s = \frac{T_{si} + T_{so}}{2}$$

where T_{fi}, T_{fo}, T_{si} and T_{so} are the inlet fluid temperature, outlet fluid temperature, inlet surface temperature and outlet surface temperature respectively.

The heat flux in the channel is given by:

$$Q_{heat} = \frac{Q_{channel}}{A_s} \tag{4}$$

where A_s is the surface area of the microchannel.

For ease of calculation and comparison of previous studies, the mass flow rate and pressure drop are converted to their respective non-dimensional forms as Reynolds number (*Re*) and friction factor (*f*) given by:

$$Re = \frac{\rho U_{avg} D_h}{\mu} \tag{5}$$

$$f = \frac{2\Delta P}{\rho U_{avg}^2 \frac{L}{D_h}} \tag{6}$$

where ρ and μ are the density and viscosity of fluid repectively. U_{avg} is the streamline velocity of fluid in flow direction and L is the length of the microchannel under test. D_h is the hydraulic diameter calculated at the charecteristic location. The viscosity of water is a function of temperature and calculated at average fluid temperature as given by Eq. 7. The average fluid temperature measured at reference temperature of 25 °C and viscosity as 8.55×10^{-4} kg/m.s.

$$\mu(T) = \mu(T_{ref}) \cdot (T/T_{ref})^{8.9} \exp\left[4700(1/T - 1/T_{ref})\right] \tag{7}$$

From previous study of Duryodhan et al. [17], the location of characteristic dimension for the diverging microchannel is at *L/3* distance from the narrow end. Similarly, the characterisic dimension for the converging microchannel is located at *L/3.6* distance from the narrow end. These characteristic dimensions are independent of *Re*, divergence or convergence angle, D_h and L. To the best of author's knowledge, not much research were carried out on location of hydraulic diameter in converging–diverging microchannels. Hence, to minimize the complications in understanding, the above characteristic location were chosen to calculate the average geometrical and flow parameters such as: hydraulic diameter (D_h), aspect ratio (γ), velocity (U_{avg}) and Reynolds number (*Re*).

To validate our findings, the experimental *f.Re* value is compared with the theoritical value calculated by Morini et al. [19]. The theoritical correlation is a function of aspect ratio (γ) given by:

$$f.\mathrm{Re} = 24 - 42.267\,\gamma^2 + 64.272\,\gamma^3 - 118.42\,\gamma^4 + 242.12\,\gamma^5 - 178.79\,\gamma^6 \tag{8}$$

Further, Nusselt number is calculated to show the heat transfer performance of the microchannels. The Nusselt number (*Nu*) is given by:

$$Nu = \frac{h_{avg} D_h}{K_f(T)} \tag{9}$$

where $K_f(T)$ is the fluid thermal conductivity calculated at average fluid temperature T_f. The thermal conductivity of fluid at a constant temperature is given by:

$$K_f(T) = (3.3 + 1.9T) \times 10^{-3} \tag{10}$$

To validate the experimental Nusselt number, the correlation from different researchers were used. Shah and London [21] used rectangular microchannels and calculated Nusselt number (as a function of aspect ratio) for a fully developed laminar flow with constant heat flux boundary condition and constant surface temperature condition as shown in Eqs. 11 and 12 respectively.

$$Nu_{\mathrm{Shah,Q}} = 8.235\left(1 - 2.0421\gamma + 3.0853\gamma^2 - 2.4765\gamma^3 + 1.0578\gamma^4 - 0.1861\gamma^5\right) \tag{11}$$

$$Nu_{\mathrm{Shah,\,T}} = 7.541\left(1 - 2.610\gamma + 4.970\gamma^2 - 5.119\gamma^3 + 2.702\gamma^4 - 0.548\gamma^5\right) \tag{12}$$

Furthermore, Lee and Garimella [22] calculated *Nu* for a thermally developing flow in rectangular microchannels with constant heat flux boundary condition as shown in Eq. 13. The flow condition used was laminar.

$$Nu = \left[1.766\left(\mathrm{Re}\,\mathrm{Pr}\,\frac{D_h}{L}\right)^{0.378}\left(\frac{H}{W}\right)^{0.1224}\right] \tag{13}$$

where *Pr* is the Prandtl number, *H* and *W* are the height and width of the microchannel respectively. *Pr* is given by:

$$Pr = \frac{\nu}{\alpha} \tag{14}$$

where ν and α are the kinematic viscosity and thermal diffusivity of the working fluid.

The uncertainity analysis in measurement data were conducted based on the procedures explained by Figliola and Beasley [23]. The uncertainity in various parameters are shown in Table 2.

Table 2 Uncertainity in experimental measurements

Parameters	Uncertainity
Mass flow rate ($\dot{m}$)	0.001232 kg/s
Pressure drop (ΔP)	0.1 psi
Electrical power (to heater)	±0.5%
Temperature	+1.5%
Heat transfer coefficient	±14%
Nusselt number	±20%
Friction factor	±9%

3 Numerical method

3.1 Numerical model and governing equations

In a microchannel system, it is important to understand the phenomenon of conjugate heat transfer as the conduction and convection takes place simulataneously. According to the literature, if the solid wall to fluid thickness goes beyond 2–3, the conjugate effect is predominant [24]. Numerical simulations were performed on the converging–diverging microchannels to estimate its increase in heat transfer coefficient. The simulations results were validated with the experimental results to analyze the predictability of the numerical methods.

A three-dimensional (3D) steady state simulation were conducted using FloEFD 15. The computational domain and boundary conditions for numerical study is shown in Fig. 5. The computational domain was set as 0.35 m × 0.35 m × 0.35 m as shown in Fig. 5a. The boundary conditions applied to the model is shown in Fig. 5b. The inset of Fig. 5b shows the distinction between the solid domain and fluid domain. Prior to assumptions on the nature of heat transfer in the computational domain, either natural convection or forced convection, evaluation of Rayleigh (*Ra*) number is mandatory [25]. The Rayleigh number is given by:

$$Ra = \frac{g\beta \Delta T L_r^3}{\nu\alpha} \tag{15}$$

where, ΔT is the temperature difference of the package and ambient. The ΔT, under maximum operating conditions, was assumed to be 100 °C, L_r is the characteristic length of the microchannel, which is 0.12 m. The other parameters were the standard thermo physical parameters of air. Solving Eq. 15 results in $Ra \approx 1.7 \times 10^7$, which was just below the typical transition value $10^8 \sim 10^9$ for the turbulent regime. Hence, natural convection under laminar flow was assumed for present numerical analysis.

The Navier–Stokes equations for the steady state conditions are: mass conservation equation, the momentum equation, and the thermal energy conservation equation as follows:

Continuity equation:

$$\frac{\partial}{\partial x}(\rho u) + \frac{\partial}{\partial y}(\rho \vartheta) + \frac{\partial}{\partial z}(\rho w) = 0. \tag{16}$$

Momentum equations:

$$\frac{\partial}{\partial x}(\rho uu) + \frac{\partial}{\partial y}(\rho vu) + \frac{\partial}{\partial z}(\rho wu) = -\frac{\partial P}{\partial x} + \mu\left(\frac{\partial^2 u}{\partial x^2} + \frac{\partial^2 u}{\partial y^2} + \frac{\partial^2 u}{\partial z^2}\right) \tag{17a}$$

$$\frac{\partial}{\partial x}(\rho uv) + \frac{\partial}{\partial y}(\rho vv) + \frac{\partial}{\partial z}(\rho wv) = -\frac{\partial P}{\partial y} + \mu\left(\frac{\partial^2 v}{\partial x^2} + \frac{\partial^2 v}{\partial y^2} + \frac{\partial^2 v}{\partial z^2}\right) \tag{17b}$$

$$\frac{\partial}{\partial x}(\rho uw) + \frac{\partial}{\partial y}(\rho vw) + \frac{\partial}{\partial z}(\rho ww) = -\frac{\partial P}{\partial z} + \mu\left(\frac{\partial^2 w}{\partial x^2} + \frac{\partial^2 w}{\partial y^2} + \frac{\partial^2 w}{\partial z^2}\right) - \rho g\,. \tag{17c}$$

Thermal energy conservation equation:For fluid:

$$\frac{\partial}{\partial x}(\rho uT) + \frac{\partial}{\partial y}(\rho vT) + \frac{\partial}{\partial z}(\rho wT) = \frac{k}{C_p}\left(\frac{\partial^2 T}{\partial x^2} + \frac{\partial^2 T}{\partial y^2} + \frac{\partial^2 T}{\partial z^2}\right) + S_e \tag{18}$$

where S_e indicates the heat source term for the radiative heat transfer which is not considered in this study.

For solid:

$$\left(\frac{\partial^2 T}{\partial x^2} + \frac{\partial^2 T}{\partial y^2} + \frac{\partial^2 T}{\partial z^2}\right) = 0. \tag{19}$$

The following assumptions and boundary conditions (as shown in Fig. 5b) were made for the simulation:

1. Fluid flow will be laminar in the computational domain.
2. All outer surfaces were adiabatic and non-radiant.
3. The process of heat transfer is under steady state condition.
4. Mass flow rate was specified as the Inlet wall boundary.
5. Outlet wall was prescribed with environmental pressure condition.
6. Constant heat flux was applied on the top surface of the microchannel.
7. Numerical simulation excludes the header. Bottom wall of microchannel was specified with adiabatic wall condition to replicate the insulated header in the experimental setup.
8. Materials assumed were homogeneous and isotropic.

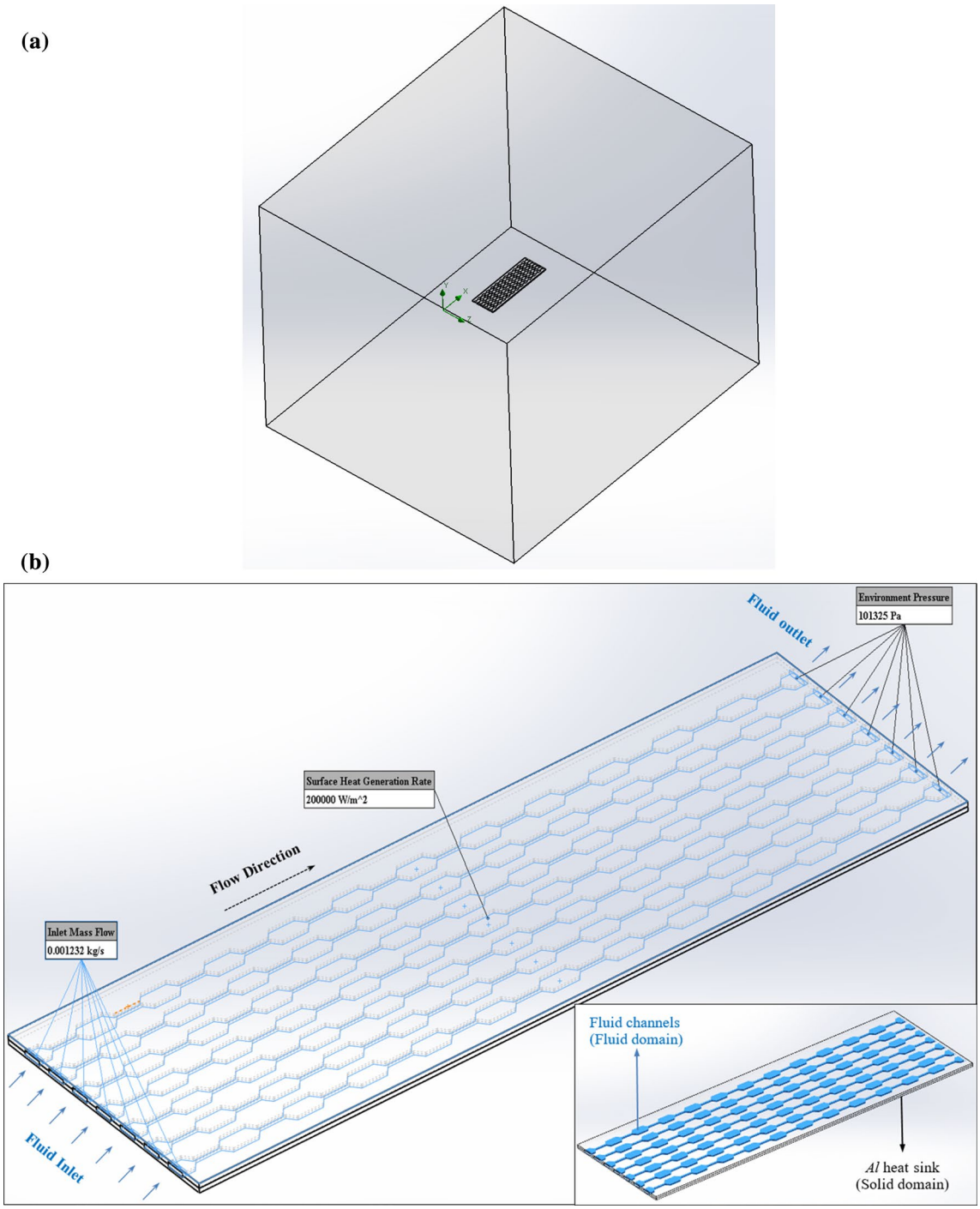

Fig. 5 **a** Computational domain and **b** boundary conditions in FloEFD 15

9. No-slip conditions were assumed at the solid–liquid bondary interface.

A Semi Implicit Method for Pressure-Linked Equations (SIMPLE) algorithm was used to couple the pressure and velocity. A second order upwind scheme was used for the discretization of the convection terms in the governing equations. In general, a relative error for the convergence criterion was considered to be less than 10^{-4}. FloEFD 15 possesses the ability for different meshing functions. In this simulation, every component in the assembly were given different meshing grids depending on the thickness of the individual layers. Table 3 shows simulation results with different number of solid cells, fluid cells and partial cells

Table 3 Grid independence

Number of cells			Avg. heat transfer coefficient (h_{avg}) (kW/m^{2}K)	% Deviation
Fluid cells	Solid cells	Total cells		
580,000	870,000	1,450,000	3.283	4.73
886200	1,223,800	2,110,000	3.446	0.55
1,090,600	1,779,400	2,870,000	3.465	

for grid independence study. From the inference, approximately 2.1 million grids were found to have good estimation [16, 26].

4 Results and discussion

4.1 Experimental results

This section focuses on the study of fluid flow and heat transfer characteristics in CD microchannel. Experimental pressure drop, temperature difference and heat transfer coefficient were calcualted in their respective non-dimensional forms. The mass flow rate and heat flux used ranges from 1.2×10^{-2} to 1.848×10^{-2} kg/s and 10–50 W/cm^2 respectively.

4.1.1 Pressure drop

Figure 6 shows the variation of pressure drop for different mass flow rate at different heat inputs. The pressure drop is measured for microchannel in non-heating (0 W) condition in order to analyze its performance at higher heat inputs. For all heat inputs, the pressure drop varies non-linearly with the increase in mass flow rate unlike in straight microchannels where pressure drop varies linearly [27]. The

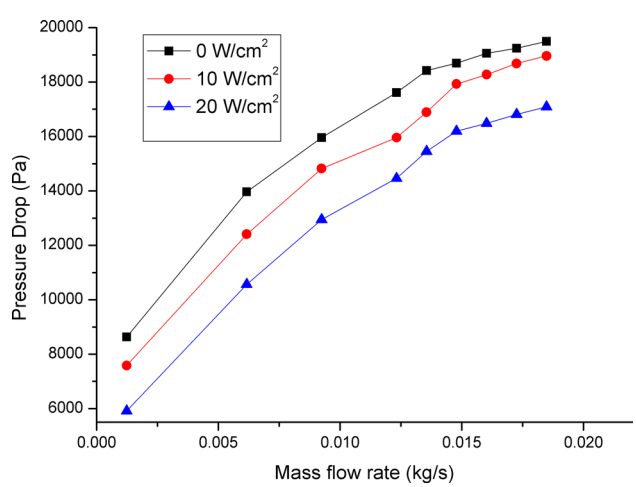

Fig. 6 Variation of pressure drop with the mass flow rate for different heat input

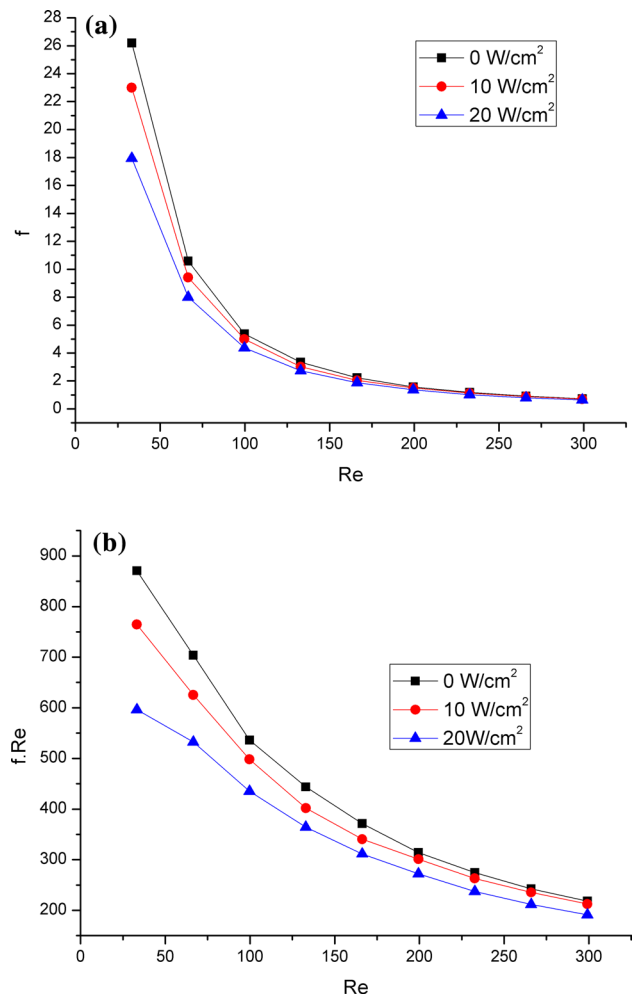

Fig. 7 Variation of **a** friction factor with Reynolds number **b** Poiseulle number with Reynolds number for different heat input

non-linearity in pressure drop suggests the influence of viscous forces over the pressure and inertial forces [17]. It also shows that the pressure drop decreases with increase in heat input. As the heat input increases, the viscosity of water decreases owing to decreased viscous forces. The reduction in viscous force reduces pressure drop adversely.

Figure 7 reveals similar findings in correlation to viscosity of water. The average fluid temperature measured at the outlet of the header were 28.3, 47.7, 61.3 °C for corresponding heat input of 10, 20 and 30 W/cm^2 respectively. The percentage reduction in viscosity can be calculated by

Eq. 7 with reference to viscosity at room temperature as already explained in Sect. 2.3. The reduction in viscosity were reported to be decreasing for increase in heat input [15]. Hence, the reduction in friction factor was almost consistent with reduction in viscosity. To validate, friction factor (f) was plotted against Reynolds number (Re) as shown in Fig. 7. Exponential decrease in curve shows the reduction in viscous force within the CD microchannel. This suggests that further investigation regarding the location of charateristic dimension is needed to normalize the friction factor.

Furthermore, Fig. 7b asserts the variation of poiseulle number ($f.Re$) with respect to theoretical correlation. The theoretical $f.Re$ calcuated from Eq. 8 is 293.65. Experimentally calculated $f.Re$ shows wide deviation to theoretical value. This is due to the fact that the theoretical value was calculated based on the aspect ratio of the microchannels measured at the characteristic dimension ($L_2/3.6$ and $L_4/3$). Whereas, the experimental $f.Re$ were calculated by the viscosity as a function of temperature. It is interesting to note that, for all the cases of heating condition as well as non-heating condition, $f.Re$ narrowed down to theoretical value for high Re. This means that, the viscous force and entrance effect of CD microchannel need to be further investigated [28]. To be noted, the error percentage on comparing the theoretical $f.Re$ to experimental $f.Re$ are 25% for non heating condition. On heating condition, the error rises to 27.7 and 34.8% for 10 and 20 W heat input respectively. It is important to note that these errors are calculated at $Re = 300$. The uncertainity in calculation of viscosity of water contributes to this error [16].

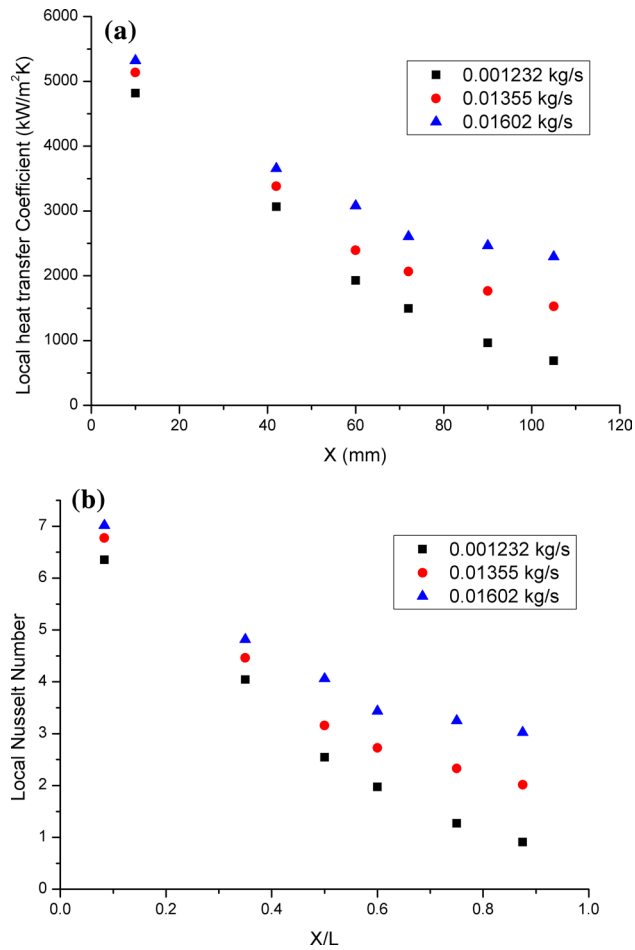

Fig. 8 Variation of **a** local heat transfer coefficient with the axial distance **b** local Nusselt number with axial distance for different mass flow rate

4.1.2 Heat transfer coefficient

Figure 8a shows the variation of local heat transfer coefficient (h_x) along the axial distance of CD microchannel. The measurements were made for three different mass flow rate: 0.001232, 0.01355 and 0.01602 kg/s. As already explained in Sect. 2, single unit of CD microchannel comprises of three different cross sections which is validated by heat transfer coefficient curve. Figure 8a shows that h_x varies non-linearly along the direction of flow in microchannel. It is interesting to note that along the straight to converging section (L_1 to L_2), h_x decreases due to decrease in Reynolds number due to change in cross-section. This happens till $[L_1 + (L_2 - L_2/3.6)]$ length of single CD microchannel unit since the flow is always in developing region for converging cross-section [17]. For L_3 in CD microchannel, h_x remains almost linear due to uniform Re. Subsequently, when there is a change in cross-section from straight-divergent in (L_3 to L_4) section, the Reynolds number increases which results in increase in h_x. It should be noted that the maximum h_x in L_5 section is lesser than in L_1 section. Over the entire length, the heat transfer coefficient reduces in comparison to the previous CD unit as acknowledged in Fig. 8a. As expected, heat transfer ability of the working fluid reduces along the length of the microchannel. In other words, h_x decreases as the fluid temperature increases. Since water is low-viscous fluid, the reduction in h_x is obvious. Additionally, when the mass flow rate were increased, the heat transfer coefficient increases along the length of the microchannel. Although, similar trend of non-linear variation in h_x were observed when mass flow rate were increased. Equivalent results were obtained for the corresponding local Nusselt number plot as shown in Fig. 8b.

Figure 9 shows the variation of average heat transfer coefficient (h_{avg}) against mass flux flow rate ($\dot{m}$). The figure shows non-linear increase in h_{avg} for the mass flux range of 0.001232–0.01848 kg/s. The heat transfer coefficient for straight microchannels increased linearly as witnessed by Kumaraguruparan et al. [27]. Aforementioned comparison supports the heat transfer trend in the CD microchannel

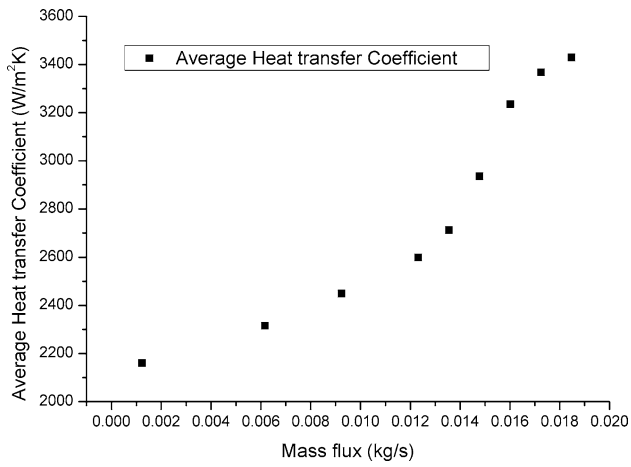

Fig. 9 Variation of average heat transfer coefficient with mass flow rate

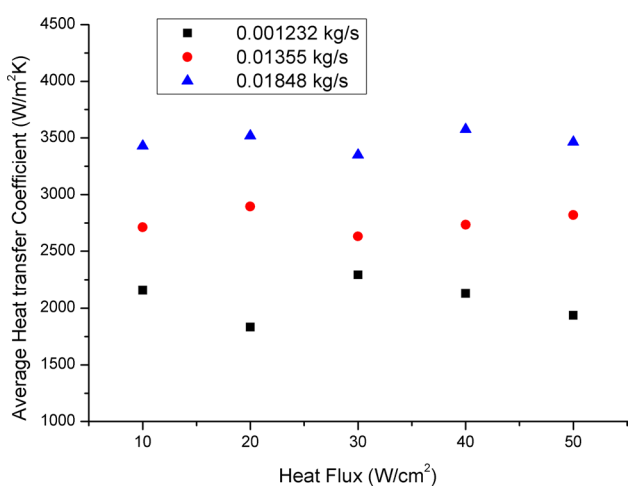

Fig. 10 Variation of average heat transfer coefficient with Input heat flux for different mass flow rate

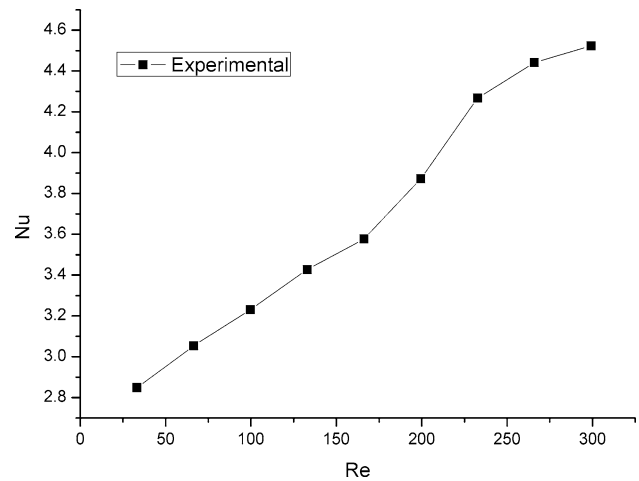

Fig. 11 Nu Vs Re plot for CD microchannel

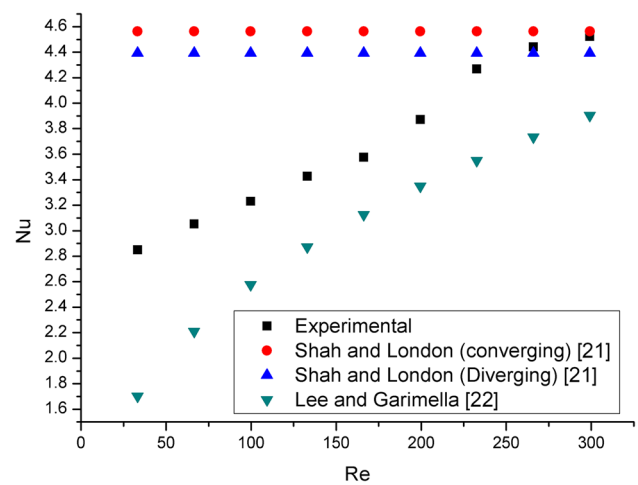

Fig. 12 Nu Vs Re correlations for CD microchannel

and conversely, it is inappropriate to compare two experimental data with dissimilar input conditions. However, it is important to understand that the straight microchannel with uniform cross-section have relatively constant flow-regime and hot solid–fluid boundary remain intact once the flow is fully developed. In case of CD microchannel, as already mentioned, the flow-regime is still in developing region. Hence, the solid–fluid boundary is constantly perturbed which results in significant thinning of hot fluid boundary adjacent to microchannel wall [13]. Therefore, CD microchannel is reported to maintain non-linear h_{avg} variation. This can be observed by Nusselt number variation as explained in next section.

In order to validate experimental data in CD microchannel, the experiments were repeated for different values of heat flux at constant mass flow rate as suggested by Duryodhan et al. [16]. Figure 10 shows the measurements taken for heat flux range of 10–50 W/cm^2 for different mass flow rates: 0.001232, 0.01355 and 0.01848 kg/s. Figure 10 also shows that the h_{avg} is independent of heat flux which were reported for conventional microchannels with uniform cross-sections. As expected in forced convection flow regime, the independence of heat transfer coefficient on heat flux was observed for CD microchannels.

4.1.3 Correlations

Figure 11 shows the variation of experimental *Nu* with *Re*. The figure shows that there is repititive linearity rather than consistent linearity in *Nu* plot unlike in straight microchannels [27]. This affirms that the converging–diverging section in CD microchannel contributes for increased *Nu*

value. The concept of solid–fluid boundary perturbation can be correlated for affirming increased *Nu* value as explained earlier [13]. To validate the above-mentioned, correlations were made in order to compare the standard results of other researchers [16].

Figure 12 shows the comparison of experimental *Nu* in this study with results from various other researchers as given in Eqs. (10–13). It should be noted that the trend is similar in all cases but the linearity differs. The two horizontal plots indicates the *Nu* calculated based on Eq. 11. The upper horizontal plot denotes the *Nu* calculated for aspect ratio at converging section (L_2) while the lower horizontal plot denotes *Nu* at diverging section (L_4) Results of Lee and Garimella was found to deviate much to CD microchannel results because it does not account for the conjage heat transfer effect [22]. The results of sole converging microchannel and diverging microchannel does not concur exactly to CD microchannel results since the cross-section was either expanding or narrowing [16]. Also the geometry of the test sections considered were different. However, the results of CD microchannel was found to establish connection with converging microchannel in early slope of *Nu* curve. This upholds the consideration of characteristic dimesion at *L/3.6* and *L/3* (from the narrow end) for the converging and diverging section respectively. Straight microchannel reported to have *Nu* value in order for 0.1–0.35 for mass flow rate ranging from 0.002 to 0.003 kg/s [27]. Experimental *Nu* value of CD microchannel shows significant increase than the straight microchannel. For correlation with equation of Shah and London [20], the experimental *Nu* value is 0.9% lower than the theoretical value calculated for aspect ratio at converging section and 3.7% higher than *Nu* calculated for aspect ratio at diverging section. For correlation with Lee and Garimella [21],

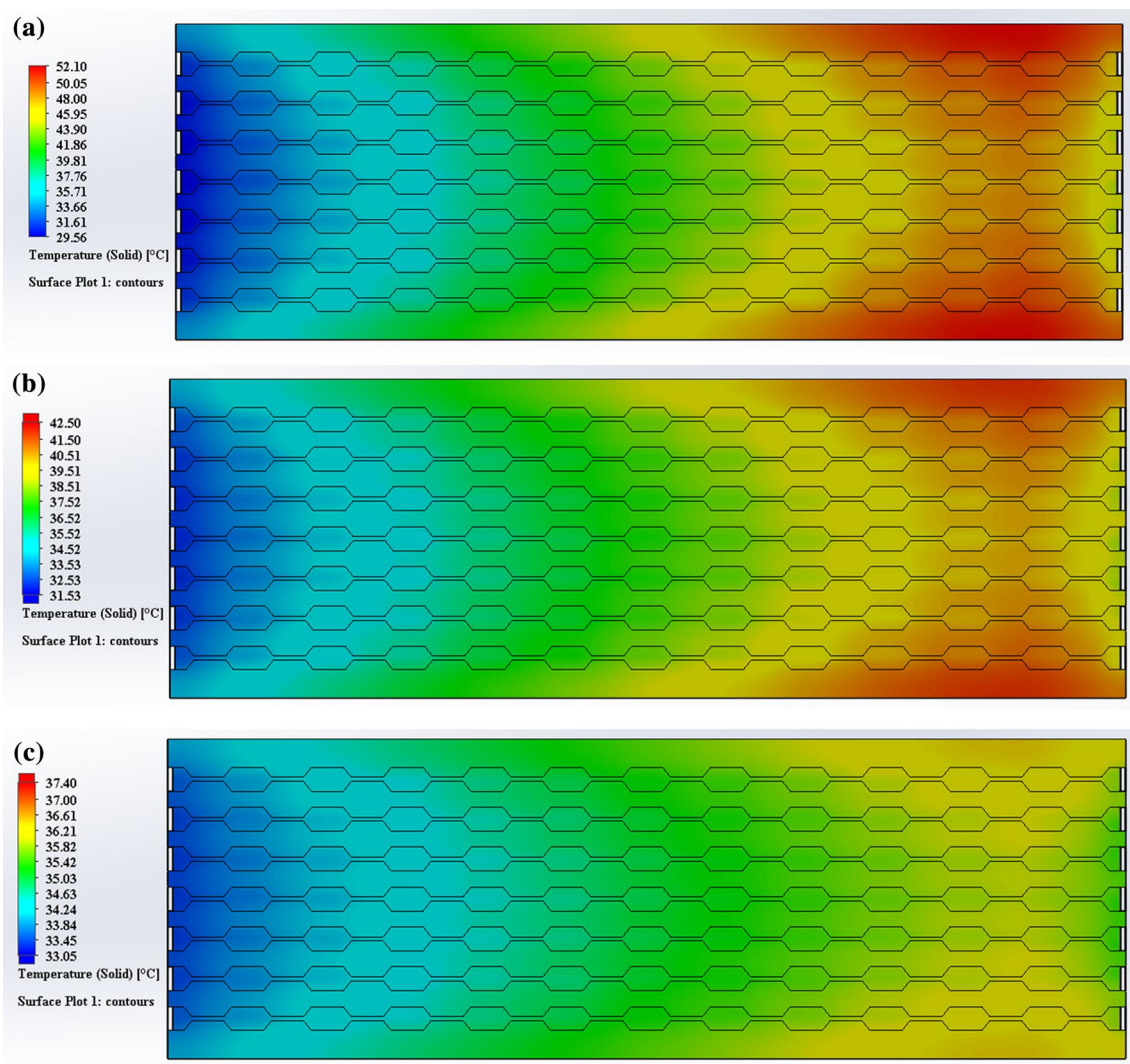

Fig. 13 Temperature distribution in CD microchannel for inlet mass flow rate of **a** 0.001232 kg/s **b** 0.01355 kg/s **c** 0.01848 kg/s

experimental *Nu* shows 15.8% higher. All these results indicates, the evaluation of heat transfer coefficients at the characteristic dimension is good for calculating the thermo-hydraulic performance of CD microchannel. Additionally it was noted, that the percentage increase in experimental *Nu* value is due to the consideration of conjugate effect in heat transfer in this study. Hence, the deviation in experimental value should not be misunderstood as error.

4.2 Numerical results

CFD simulation was conducted by specifying the boudary conditions as explained in Sect. 3.1. Initially, the simulations were commenced for the standard geometries and unifrom cross-section microchannels for which the results were known. This was done to validate the numerical results. Further, the numerical simulations were done for CD microchannels that replicates the experimental conditions. Figure 13 shows the temperature distribution in CD microchannel. As it is colossal to present data for all the cases studied, results of microchannel subjected to uniform heat flux of 20 W/cm^2 and three mass flow rates: 0.01232 kg/s, 0.01355 kg/s and 0.01848 kg/s were shown in Fig. 13(a–c) respectively. Apparently, the surface temperature of the heat sink reduces due to superior thermal performance in CD section. At low mass flow rate, the surface temperature was high at the outlet end of the microchannel as shown in Fig. 13a. As the mass flow rate increases, the kinetic energy of the fluid increases resulting in enhanced heat transfer in microchannel. As an effect, the surface temperature of the CD microchannel heat sink becomes almost uniform barring the surface near outlet as shown in Fig. 13c [18]. The Nusselt number can be calculated from the numerical data using Eq. 9. The average Nusselt number computed was plotted against the Reynolds numbers for experimental results and numerical results as shown in Fig. 14. From the figure, it was observed that the experimental results and simulation predictions were in good agreement. The maximum error was observed to be 7.8% which was due to experimental uncertainities. Henceforth, the simulation data appears to be a valuable resource in predicting the experimental results [24].

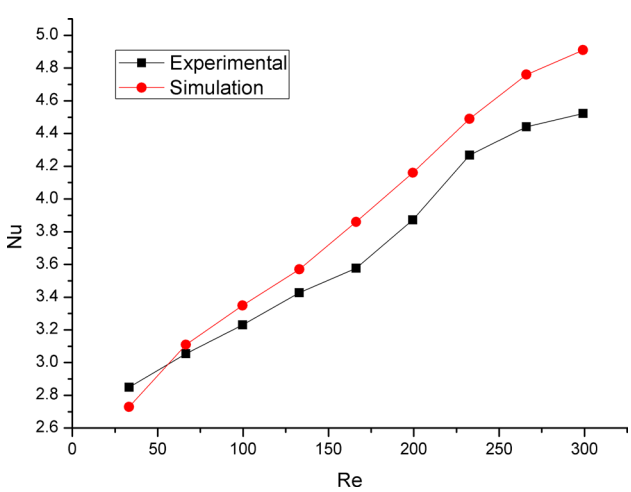

Fig. 14 Comparison of Nu Vs Re obtained from experiment and simulation

5 Conclusions

Microchannels with varying cross-section are being extensively used for cooling in this study. Converging–diverging microchannels were fabricated on Aluminium heat sink using micro milling technique. Experimental and three dimensional CFD investigations were carried out for CD microchannels. Experimental setup was created and measurements were conducted for mass flow rate ranging from 0.001232 to 0.01848 kg/s and heat flux ranges of 10–50 W/cm^2. Pressure drop and heat transfer coefficients were measured for the subjected experiments. On experiments, it was found that the pressure drop in CD microchannels vary linearly while the friction factor observed to decrease due to the influence of viscous forces. The heat transfer coefficient was detected to be higher than the straight microchannel. Re-circulation zones in CD microchannel enhances the perturbation of solid–fluid boundary in the channel wall to enhance the heat transfer coefficient. The predicted Nusselt number affirms the same. On further correlations, theoretical *Nu* decreased 0.9% and increased 3.7% when the aspect ratio was measured at converging section and diverging section respectively. Also, the experimental *Nu* was 15.8% higher than parallel microchannels. Numerical simulations were performed for similar experimental conditions in order to validate the measurement data. Numerical results adheres to experimental measurements and found to have maximum error of 8%. Therefore, CD microchannels exhibits better thermal–hydraulic performace than the straight microchannels. This affirms the application of CD microchannels in thermal management of microdevices.

Acknowledgements The author gratefully acknowleges Institute of Post-graduate Studies, Universiti Sains Malaysia for financal assistance through USM Fellowship.

References

1. Tuckerman DB, Pease FW (1981) High-performance heat sinking for VLSI. IEEE Electron Device Lett 2(5):126–129
2. Singh SG, Agrawal A, Duttagupta SP (2011) Reliable MOSFET operation using two-phase microfluidics in the presence of high heat flux transients. J Micromech Microeng 21(10):105002
3. Singh SG, Duttagupta SP, Agrawal A (2009) In situ impact analysis of very high heat flux transients on nonlinear pn diode

characteristics and mitigation using on-chip single-and two-phase microfluidics. J Microelectromech Syst 18(6):1208–1219
4. Wu HY, Cheng P (2003) An experimental study of convective heat transfer in silicon microchannels with different surface conditions. Int J Heat Mass Transf 46(14):2547–2556
5. Geyer PE, Rosaguti NR, Fletcher DF, Haynes BS (2006) Thermohydraulics of square-section microchannels following a serpentine path. Microfluid Nanofluid 2(3):195–204
6. Sui Y, Teo CJ, Lee PS, Chew YT, Shu C (2010) Fluid flow and heat transfer in wavy microchannels. Int J Heat Mass Transf 53(13):2760–2772
7. Lee PC, Pan C (2007) Boiling heat transfer and two-phase flow of water in a single shallow microchannel with a uniform or diverging cross section. J Micromech Microeng 18(2):025005
8. Agrawal A, Duryodhan VS, Singh SG (2012) Pressure drop measurements with boiling in diverging microchannel. Front Heat Mass Transf (FHMT) 3:013005
9. Koşar A, Peles Y (2006) Thermal-hydraulic performance of MEMS-based pin fin heat sink. J Heat Transf 128(2):121–131
10. Peles Y, Koşar A, Mishra C, Kuo CJ, Schneider B (2005) Forced convective heat transfer across a pin fin micro heat sink. Int J Heat Mass Transf 48(17):3615–3627
11. Rahman MM (2000) Measurements of heat transfer in microchannel heat sinks. Int Commun Heat Mass Transf 27(4):495–506
12. Rosaguti NR, Fletcher DF, Haynes BS (2006) Laminar flow and heat transfer in a periodic serpentine channel with semi circular cross section. Int J Heat Mass Transf 49:2912–2923
13. Gong L, Kota K, Tao W, Joshi Y (2011) Parametric numerical study of flow and heat transfer in microchannels with wavy walls. J Heat Transf 133(5):051702
14. Xuan X, Li D (2005) Particle motions in low-Reynolds number pressure-driven flows through converging–diverging microchannels. J Micromech Microeng 16(1):62
15. Louisos WF, Hitt DL (2007) Heat transfer and viscous effects in 2D and 3D micronozzles. In: 37th AIAA fluid dynamics conference, 3987, pp 1–17
16. Duryodhan VS, Singh A, Singh SG, Agrawal A (2015) Convective heat transfer in diverging and converging microchannels. Int J Heat Mass Transf 80:424–438
17. Duryodhan VS, Singh SG, Agrawal A (2013) Liquid flow through a diverging microchannel. Microfluid Nanofluid 14(1–2):53–67
18. Duryodhan VS, Singh A, Singh SG, Agrawal A (2016) A simple and novel way of maintaining constant wall temperature in microdevices. Sci Rep 6:18230. doi:10.1038/srep18230
19. Yong JQ, Teo CJ (2014) Mixing and heat transfer enhancement in microchannels containing converging-diverging passages. J Heat Transf 136(4):041704
20. Morini GL (2004) Laminar liquid flow through silicon microchannels. J Fluids Eng 126(3):485–489
21. Shah RK, London AL (1978) Lanimar flow forced convection in duts: a source book for compact heat exchanger analytical data. Academic press, Cambridge
22. Lee PS, Garimella SV (2008) Saturated flow boiling heat transfer and pressure drop in silicon microchannel arrays. Int J Heat Mass Transf 51(3):789–806
23. Figliola RS, Beasley D (2015) Theory and design for mechanical measurements. Wiley, Hoboken
24. Maranzana G, Perry I, Maillet D (2004) Mini-and micro-channels: influence of axial conduction in the walls. Int J Heat Mass Transf 47(17):3993–4004
25. Raypah ME, Dheepan MK, Devarajan M, Sulaiman F (2016) Investigation on thermal characterization of low power SMD LED mounted on different substrate packages. Appl Thermal Eng 101:19–29
26. Patankar S (1980) Numerical heat transfer and fluid flow. CRC Press, Boca Raton
27. Kumaraguruparan G, Sornakumar T (2010) Development and testing of aluminum micro channel heat sink. J Thermal Sci 19(3):245–252
28. Morini GL, Yang Y (2013) Guidelines for the determination of single-phase forced convection coefficients in microchannels. J Heat Transf 135(10):101004